Supporting Information

Selective recognition of *c-MYC* Pu22 G-quadruplex by a fluorescent probe

Qianqian Zhai [1,2] †, Chao Gao [3] ,† , Jieqin Ding [2],†, Yashu Zhang [3], Barira Islam [4], Wenxian Lan [5], Haitao Hou [2], Hua Deng [2], Jun Li [2], Zhe Hu [1], Hany I. Mohamed [2,6],Shengzhen Xu [2], Chunyang Cao [5], Shozeb M. Haider [4] and Dengguo Wei [1,2]*

[1] State Key Laboratory of Agricultural Microbiology, Huazhong Agricultural University, Wuhan 430070, PR China

[2] College of Science, Huazhong Agricultural University, Wuhan 430070, China.

[3] College of Plant Science and Technology, Huazhong Agricultural University, Wuhan 430070, PR China

[4] UCL School of Pharmacy, University College London, 29-39 Brunswick Square, London WC1N 1AX, U.K.

[5] State Key Laboratory of Bioorganic and Natural Products Chemistry and Collaborative Innovation Center of Chemistry for Life Sciences, Shanghai Institute of Organic Chemistry, Chinese Academy of Sciences, 345 Lingling Road, Shanghai, 200032, China

[6] Chemistry Department, Faculty of Science, Benha University, Benha 13518, Egypt

Table S1. DNA and RNA sequences used in the fluorescence intensity measurement

Name	**Type/origin**	**Structure**	**Sequence(5'→3')**
DNA G-quadruplex forming oligonucleotide sequences			
Bom17	G4-Bombyx telomere	Antiparallel	GGTTAGGTTAGGTTAGG
Asc20	G4-Ascaris telomere	Antiparallel	GGCTTAGGCTTAGGCTTAGG
CT4	G4/Mixed quartets	Antiparallel	GGGCTTTTGGGC
TBA	G4-Aptamer	Antiparallel	GGTTGGTGTGGTTGG
21CTA	G4-Human telomere	Antiparallel	GGGCTAGGGCTAGGGCTAGGG
c-MYC Pu22	G4-Promoter	Parallel	TGAGGGTGGGTAGGGTGGGTAA
c-KIT 1	G4-Promoter	Parallel	AGGGAGGGCGCTGGGAGGAGGG
c-KIT 2	G4-Promoter	Parallel	GGGCGGGCGCGAGGGAGGGG
Kras	G4-Promoter	Parallel	GGGCGGTGTGGGAAGAGGGAAGAGGGG
VEGF	G4-Promoter	Parallel	CGGGGCGGGCCTTGGGCGGGGT
AKT1	G4-Promoter	Parallel	GGGCGGGCGGCTCCGGGCGCGGG
TTA	G4-Human DNA	Mixed	GGGTTAGGGTTAGGGTTAGGG
TTA 45	G4-Human DNA	Mixed	GGGTTAGGGTTAGGGTTAGGGTTAGGGTTAGGG
Plas24	G4-Plasmodium	Mixed	GGGTTCAGGGTTCAGGGTTCAGGG
DNA Non-G-quadruplex forming oligonucleotide sequences			
CGG12	Trinucleotide	Trinucleotide	CGGCGGCGGCGGCGGCGGCGGCGGCGGCG
19AT	Duplex	Duplex	ACGTCGATTATAGACGAGC
19AT-			GCTCGTCTATAATCGACGT
dT30	Single strand	Single strand	TTTTTTTTTTTTTTTTTTTTTTTTTTTTTT
Triplex	Triplex	Triplex	(a) TTTTTTTTTTTTTTTTTTTT
			(b) AAAAAAAAAAAAAAAAAAAA
			(c) TTTTTTTTTTTTTTTTTTTT
Wild-type G-quadruplex forming sequences in the promoter region *of c-MYC*			
c-MYC Pu18	G4-Promoter	Parallel	AGGGTGGGGAGGGTGGGG
c-MYC Pu24	G4-Promoter	Parallel	TGAGGGTGGGGAGGGTGGGGAAGG
c-MYC Pu27	G4-Promoter	Parallel	TGGGGAGGGTGGGGAGGGTGGGGAAGG
RNA G-quadruplex forming oligonucleotide sequences			
ADAM10	G4-5′-UTR	Parallel	GGGGGACGGGUAGGGGCGGGAGGUAGGGG
ERSI	G4-5′-UTR	Parallel	GGGUAGGGGCAAAGGGGCUGGGG
TRF2	G4-5′-UTR	Parallel	CGGGAGGGCGGGGAGGGC
ZIC1	G4-5′-UTR	Parallel	GGGUGGGGGGGGCGGGGGAGGCCGGGG
BCL-2	G4-5′-UTR	Parallel	AGGGGGCCGUGGGGUGGGAGCUGGGG
VEGF	G4-5′-UTR	Parallel	GGAGGAGGGGGAGGAGGA
Tel22	G4-TERRA	Antiparallel	AGGGUUAGGGUUAGGGUUAGGG
KRAS	G4-5′-UTR	Parallel	UGGCGGCGGCGAAGGU

Table S2. Excitation wavelength and emission wavelength of compounds 1-25

Compounds	**1**	**2**	**3**	**4**	**5(9CI)**	**6**	**7**	**8**	**9**
E_{ex}/nm	308	378	298	305	405	307	379	366	277
E_{em}/nm	468	522	431	471	472	484	492	422	417

Compounds	**10**	**11**	**12**	**13**	**14**	**15**	**16**	**17**	**18**
E_{ex}/nm	356	334	365	310	348	310	308	305	361
E_{em}/nm	438	439	438	450	440	460	440	460	444

Compounds	**19**	**20**	**21**	**22**	**23**	**24**	**25**		
E_{ex}/nm	329	303	357	345	355	349	305		
E_{em}/nm	442	419	473	415	443	452	431		

Table S3. Sequences of the oligonucleotides used in imaging AS1411

Name	**Sequence(5’-3’)**
c-MYC Pu22-MFP	TGAGGGTGGGTAGGGTGGGTAAAAAAAATGAGGGTGGGTAGGGTGGGTAAAAAAAATGCCTGCGAGA
TTA2-MFP	GGGTTAGGGTTAGGGTTAGGGAAAAAAGGGTTAGGGTTAGGGTTAGGGAAAAAATGCCTGCGAGA
AS1411-M	GGTGGTGGTGGTTGTGGTGGTGGTGGAAAAAATCTCGCAGGCA

Scheme S1. Synthesis route of 9CI (compound 5) and compound 6.

Figure S1. Structures of compounds 10-25 and their fluorescent response.

Figure S2 Fluorescence responses of 9Cl (0.5 μM) in the presence of various RNA G-quadruplex. The concentration of RNA G-quadruplex is 0.5 μM. The samples were prepared in the buffer containing 10mM K_2HPO_4/KH_2PO_4 with 100mM KCl at pH 7.0

Figure S3. Predicted binding conformations of compound 1 (A) and 2 (B) at the 3' end cleft of *c-MYC* Pu22 G-quadruplex structure. Fluorophores in these two compounds are colored in purple**.**

Figure S4. A) ^{1}H NMR spectrum of 9Cl (compound 5); B) ^{13}C NMR spectrum of 9Cl; C) HRMS of 9Cl.

Figure S5. A) ^{1}H NMR spectrum of Compound 6; B) ^{13}C NMR spectrum of Compound 6; C) HRMS of Compound 6.

Figure S6. (A) Absorption spectra of 5 μM 9CI in the buffer (10 mM K_2HPO_4/KH_2PO_4, pH 7.0, 100 mM KCl), (B) absorption spectra of 0.5 μM 9CI in the presence of 0.5 μM *c-MYC* Pu22 DNA oligonucleotide, (C) fluorescence spectra of 9CI (0.5 μM) in the absence and the presence of *c-MYC* Pu22 DNA oligonucleotide (3 eq. to 9CI) with the excitation wavelength at 405 nm.

Figure S7. Linear fit equations for calculating the limits of detection (LOD) values of compound 9CI (0.5 μM) for *c-MYC* Pu22 G-quadruplex forming DNA oligonucleotide in buffer (10 mM K_2HPO_4/KH_2PO_4, pH 7.0, 100 mM KCl) at room temperature (λ_{ex} = 405 nm, λ_{em} = 472 nm).

Figure S8. Cytotoxicity effect of 9CI on A549 cells.

Figure S9. Fluorescence response of 0.5 μM 9CI and mixture (0.5 μM *c-MYC* Pu22 and 0.5

μM 9CI) in buffer and cell lysate at Ex = 405 nm. Buffer: 10 mM K_2HPO_4/KH_2PO_4, 100 mM KCl pH 7.0; cell lysate: 30000 cells/mL of A549 in solution (10 mM K_2HPO_4/KH_2PO_4, 100 mM KCl pH 7.0).

Figure S10. Fluorescence images of A549 cells transfected with 40 pmol labelled TTA G-quadruplex forming oligonucleotide using lipofectamine 2000, and then incubated with 5μM 9Cl for 2 hours. (A) Fluorescence signal collected between 655-755 nm at λ_{ex} = 635 nm, (B) fluorescence signal collected between 425-470nm at λ_{ex} = 405 nm, (C) fluorescence signal collected between 500-545nm at λ_{ex} = 405 nm, (D) merged image of (B) and (C). (E) merged images of (A), (B), (C) and bright field. Scale bar, 20 μm.

Figure S11. Fluorescence images of A549 cells transfected with 40 pmol labelled *c-KIT*1 G-quadruplex forming oligonucleotide using lipofectamine 2000, and then incubated with 5 μM 9Cl for 2 hours. (A) Fluorescence signal collected between 655-755 nm at λ_{ex} = 635 nm, (B) fluorescence signal collected between 425-470nm at λ_{ex} = 405 nm, (C) fluorescence signal collected between 500-545 nm at λ_{ex} = 405 nm, (D) merged image of (B) and (C), (E) merged images of (A), (B), (C) and bright field. Scale bar, 20 μm.

Figure S12. Fluorescence images of A549 cells transfected with 40 pmol *c-MYC* Pu22 G-quadruplex forming oligonucleotide labelled with Cy3 using lipofectamine 2000, and then incubated with 5 μM 9Cl for 2 hours. (A) Fluorescence signals at λ_{ex} = 405 nm, λ_{em} = 500-545 nm; (B) fluorescence signals at λ_{ex} = 405 nm, λ_{em} = 570-625nm (Cy3); (C) merged image of (A),(B) and bright field; (D) image of 9CI prior to photobleaching of the acceptor Cy3 (insert), (E) the fluorescence enhancement of 9CI after Cy3 was photobleached (insert), (F) FRET efficiency measured with the donor quenching approach，and the color bar represents the FRET efficiency. Scale bar, 10 μm.

Figure S13. Fluorescence spectra of solution at λ_{ex} = 405 nm.1) 1 μM 9CI (black line); 2) 1 μM 9CI and 0.5 μM *c-MYC* Pu22 DNA (red line); 3) 1 μM 9CI, 0.5 μM *c-MYC* Pu22-MFP

DNA and 0.5 μM SL1-M (blue line).

Figure S14. Confocal microscopy images of the treated A549 cells and HEK293T cells at 405 nm excitation. Cells was incubated with AS1411-M for 30 min at room temperature, and washed by 1 mL DPBS twice. Then, the cells were incubated with 500 nM MFP (*c-MYC* Pu22-MFP/ TTA-MFP) and 5μM 9CI for 10 min. Fluorescence signals were collected after the cells were washed with DPBS three times again. (A) Fluorescence signals collected at 425-470 nm emission channel, (B) fluorescence signals collected at 500-545 nm emission channel, (C) merged image of (A) and (B) and bright field. Scale bar, 10 μm.

Figure S15. Job plot analysis for the binding stoichiometry of 9CI to *c-MYC* Pu22 G-quadruplex in 10 mM KH_2PO_4/K_2HPO_4 buffer (pH 7.0) with 100 mM KCl at room temperature. The sum of the concentration of 9CI and the concentration of *c-MYC* Pu22 G-quadruplex-forming oligonucleotide was fixed at 2 μM. The fluorescence intensity was plotted against molar ratio of [9CI]/([9CI] + [DNA]). The excitation wavelength was set at 405 nm, and the emission was collected at 472 nm. The intersection point is near 0.5, where 9CI exhibits binding of 1:1 stoichiometry to *c-MYC* Pu22 G-quadruplex.

Figure S16. ITC binding isotherm of 20 μM 9CI interacting with 150 μM *c-MYC* Pu22 G-quadruplex DNA. This experiment was performed in buffer with 100 mM KCl, 10 mM KH_2PO_4/K_2HPO_4 (pH 7.0) at 25 ^{o}C.

Figure S17. Linear relationship of fluorometric titration. Benesi-Hildebrand plot of $1/(F-F_0)$ versus 1/[DNA]. The Ka value was calculated as 8.33×10^5 M^{-1} for the binding between *c-MYC* Pu22 G-quadruplex and 9CI.

Figure S18. CD spectra of 10 μM G-quadruplex-forming oligonucleotides *c-MYC* Pu22, *c-KIT1*, TTA, TBA and CT4 in 10 mM KH_2PO_4/K_2HPO_4 buffer, 100 mM KCl, pH 7.0, with/without 20 μM 9CI at room temperature.

Figure S19. CD spectra of 10 μM *c-MYC* Pu22 DNA G-quadruplex oligonucleotide and the mutated oligonucleotides: *c-MYC* Pu22 G2>C2, *c-MYC* Pu22 T11>A11, *c-MYC* Pu22 T20>A20, *c-MYC* Pu22 A22>T22, *c-MYC* Pu22 A3>T3, *c-MYC* Pu22 G10>T10 in 10 mM KH_2PO_4/K_2HPO_4 buffer, 100 mM KCl, pH 7.0, with/without 20 μM 9CI at room temperature.

Figure S20. Binding model of 9CI in the 3' end cleft of *c-MYC* Pu22 G-quadruplex as predicted by Autodock 4.0. G-quadruplex is in yellow stick, and 9CI is in green. Figure B was obtained by rotating 90^o from Figure A.

Figure S21. (A) RMSD of nucleic acid backbone in *c-MYC* Pu22 G-quadruplex structure over the course of the molecular dynamic simulation between 9CI and *c-MYC* Pu22 G-quadruplex. The inset structures highlight the conformation of binding at 100ns, 300ns, 500ns, 700ns and 1000ns. (B) Distance between C1' atoms of G19 and T20; (C) distance between C1' atoms of T20 and A22. (D) Conformational flexibility of the T20-A21-A22 loop observed over the course of the simulation. The figure illustrates 20 structures extracted every 50 ns. The conformation of the ligand (yellow) and the rest of the G-quadruplex is a snapshot taken at 1000 ns.

Figure S22. Binding modes of 9CI in the 3' end cleft of *c-MYC* Pu22 G-quadruplex explored by molecular dynamics simulation. Three figures are in different orientation.

Figure S23. Fluorescence intensity variance of 9CI (1 μM) in buffer (10mM K_2HPO_4/KH_2PO_4 with 100 mM KCl at pH 7.0) with glycerol at different concentrations.

Figure S24. 1D ^1H NMR spectra of *c-MYC* Pu22 G-quadruplex DNA mixing with d6-DMSO at different ratios (V/V).

Scheme S1. Synthesis route of 9Cl (compound 5) and compound 6

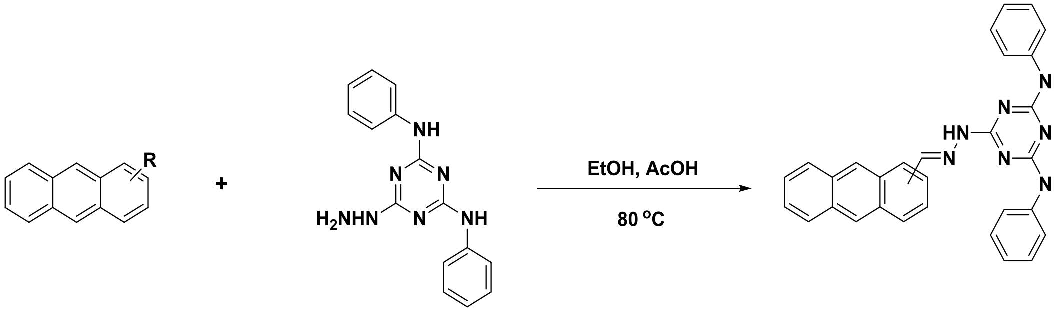

I

II

9Cl (Compound 5) and Compound 6

9Cl (Compound 5): I= anthracene-9-carbaldehyde

Compound 6: I= anthracene-2-carbaldehyde

Figure S1. Structures of compounds 10-25 and their fluorescent response to eighteen DNA oligonucleotides[a].

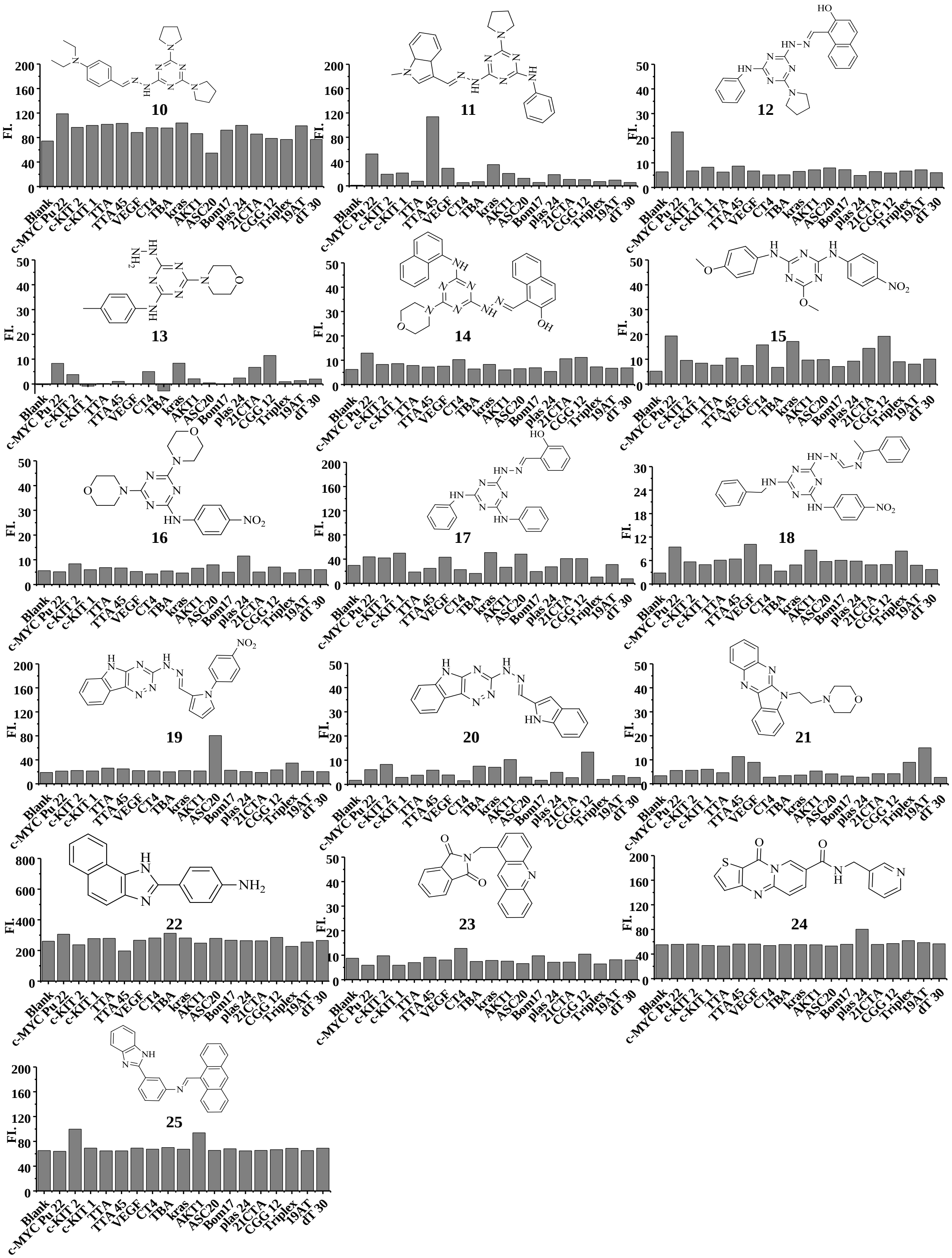

[a] The excitation and emission wavelengths of these compounds are listed in Table S2.

Figure S2. Fluorescence responses of 9Cl (0.5 μM) in the presence of various RNA G-quadruplex forming oligonucleotides (Table S1). The concentration of RNA G-quadruplex is 0.5 μM. The samples were prepared in the buffer containing 10 mM K_2HPO_4/KH_2PO_4 with 100 mM KCl at pH 7.0.

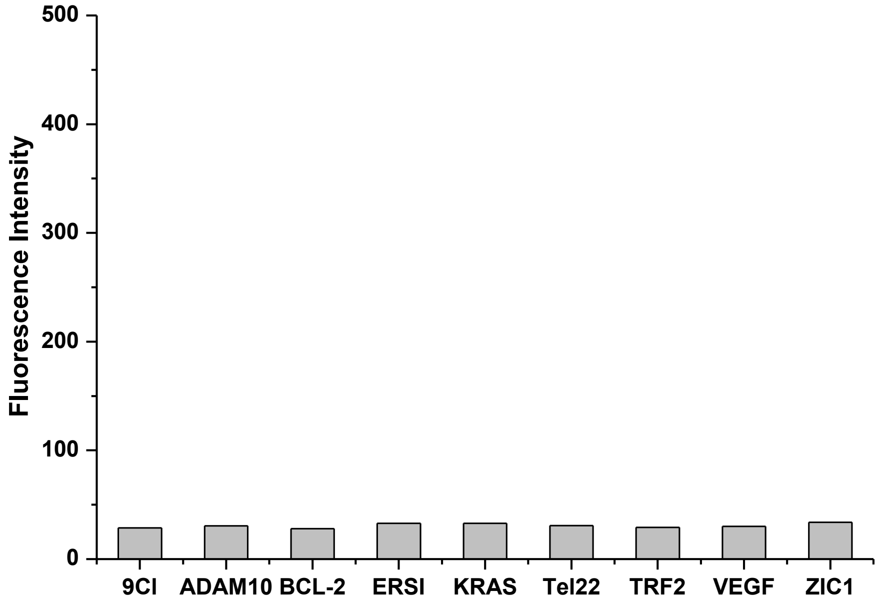

Figure S3. Predicted binding conformations of compound 1 (A) and 2 (B) at the 3' end cleft of *c-MYC* Pu22 G-quadruplex structure. Fluorophores in these two compounds are colored in purple**.**

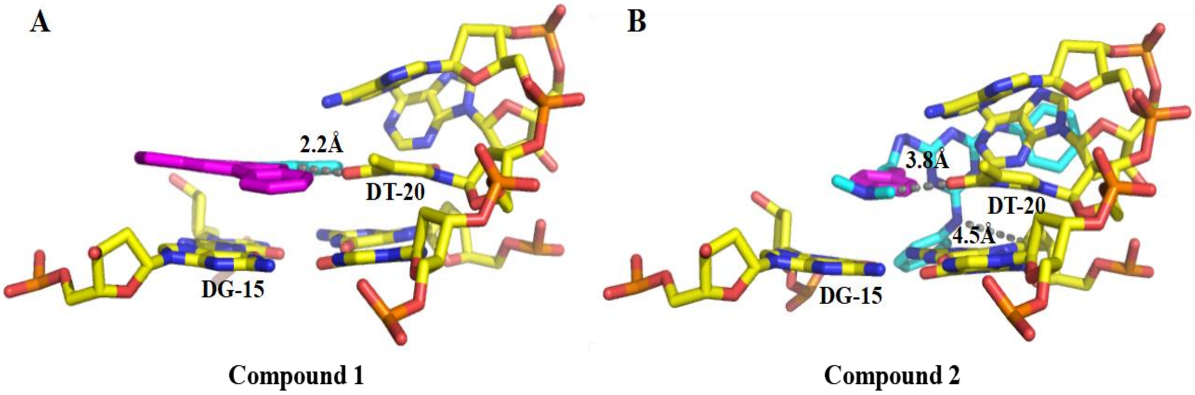

Figure S4. A) ^{1}H NMR spectrum of 9Cl (compound 5); B) ^{13}C NMR spectrum of 9Cl; C) HRMS of 9Cl.

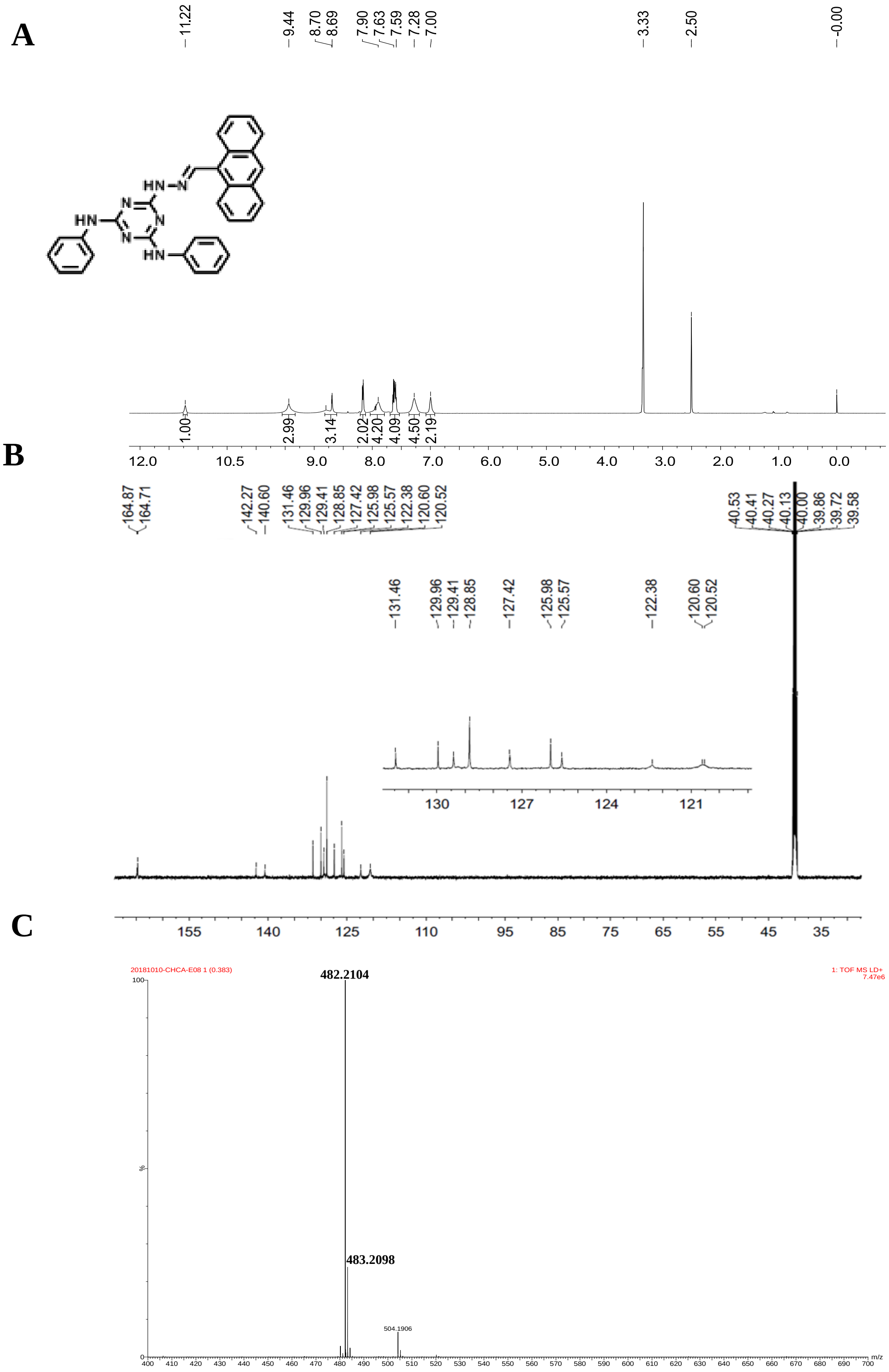

Figure S5. A) ^{1}H NMR spectrum of Compound 6; B) ^{13}C NMR spectrum of Compound 6; C) HRMS of Compound 6.

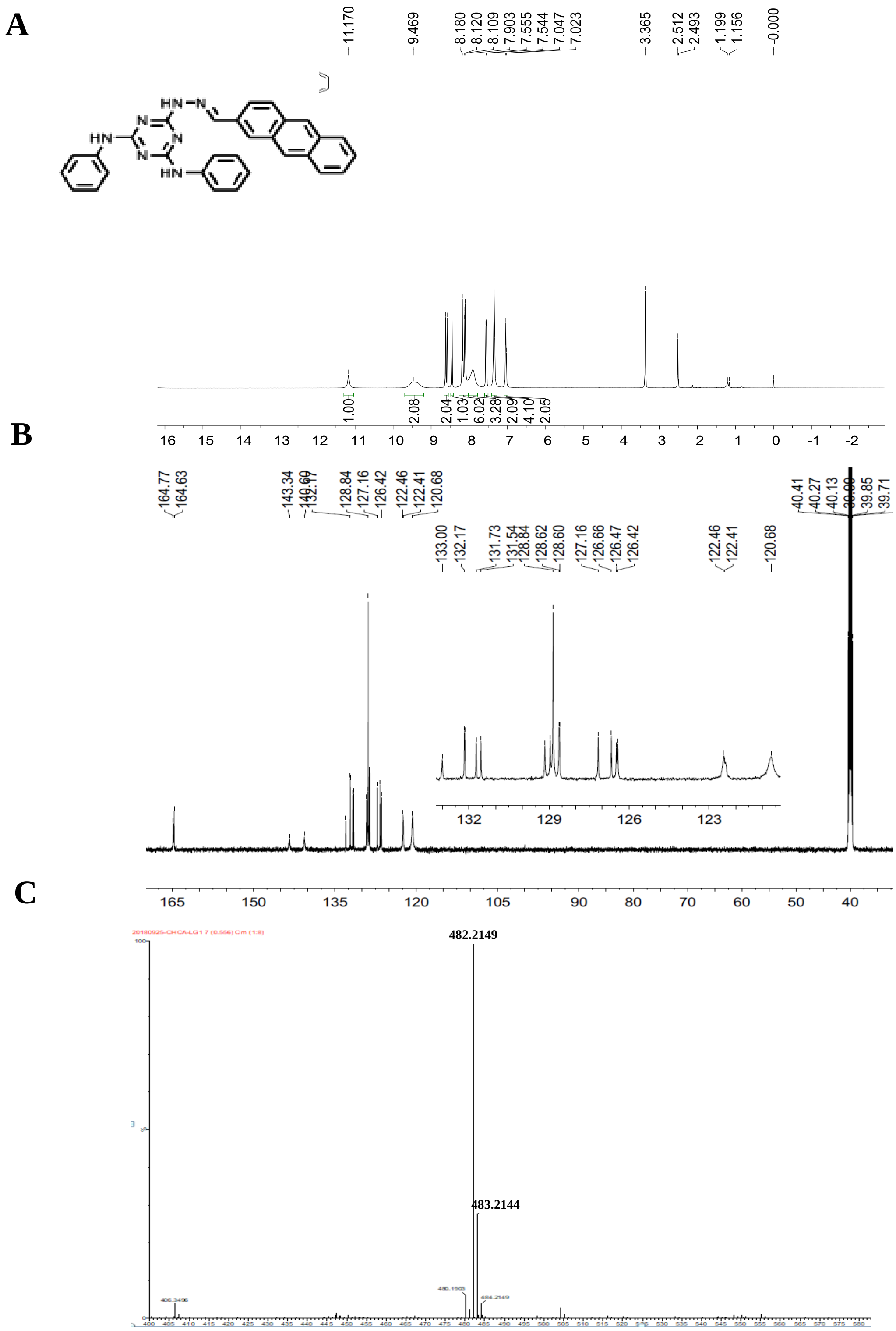

Figure S6. (A) Absorption spectra of 5 μM 9CI in the buffer (10 mM K_2HPO_4/KH_2PO_4, pH 7.0, 100 mM KCl), (B) absorption spectra of 0.5 μM 9CI in the presence of 0.5 μM *c-MYC* Pu22 DNA oligonucleotide, (C) fluorescence spectra of 9CI (0.5 μM) in the absence and the presence of *c-MYC* Pu22 DNA oligonucleotide (3 eq. to 9CI) with the excitation wavelength at 405 nm.

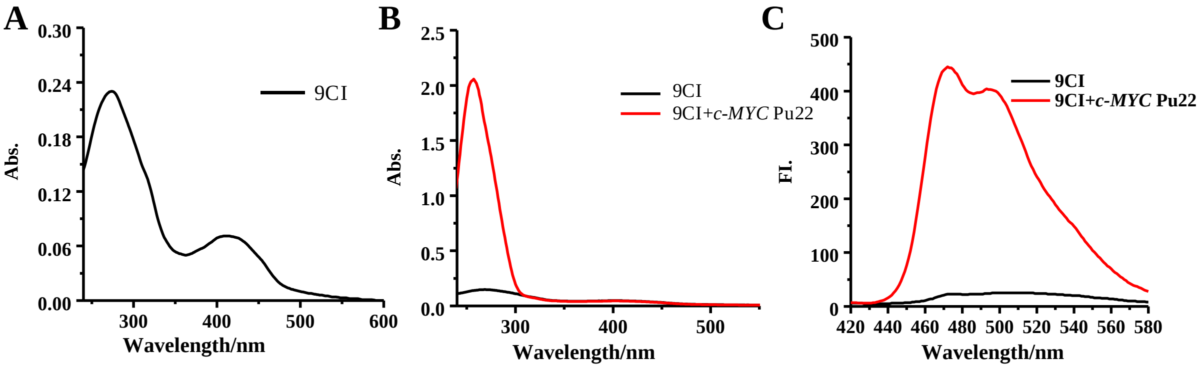

Figure S7. Linear fit equations for calculating the limits of detection (LOD) values of compound 9CI (0.5 μM) for *c-MYC* Pu22 G-quadruplex forming DNA oligonucleotide in buffer (10 mM K_2HPO_4/KH_2PO_4, pH 7.0, 100 mM KCl) at room temperature (λ_{ex} = 405 nm, λ_{em} = 472 nm).

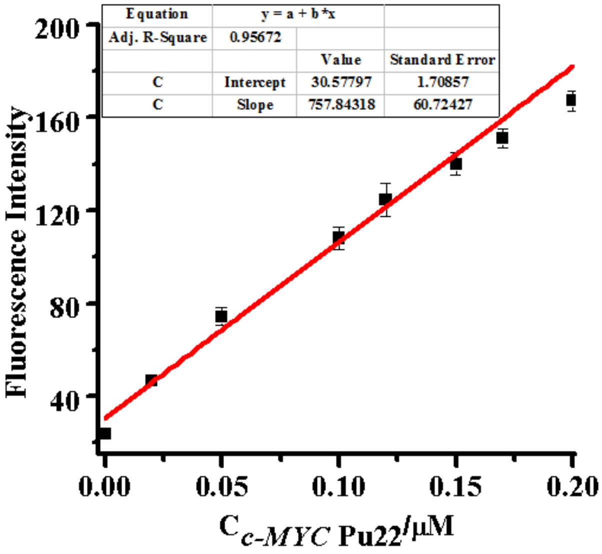

Equation	y = a + b*x		
Adj. R-Square	0.95672		
		Value	Standard Error
C	Intercept	30.57797	1.70857
C	Slope	757.84318	60.72427

Figure S8. Cytotoxicity effect of 9CI on A549 cells.

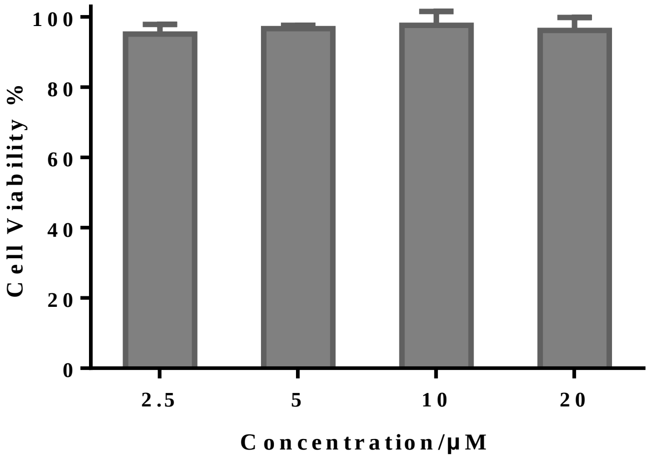

Figure S9. Fluorescence response of 0.5 μM 9CI and mixture (0.5 μM *c-MYC* Pu22 and 0.5 μM 9CI) in buffer and cell lysate at Ex = 405 nm. Buffer: 10 mM K_2HPO_4/KH_2PO_4, 100 mM KCl pH 7.0; cell lysate: 30000 cells/mL of A549 in solution (10 mM K_2HPO_4/KH_2PO_4, 100 mM KCl pH 7.0).

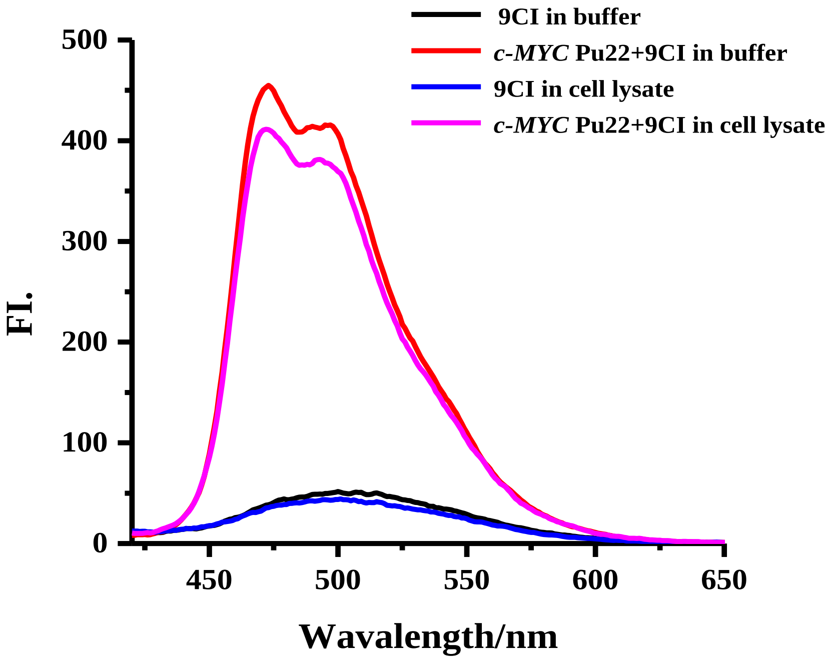

Figure S10. Fluorescence images of A549 cells transfected with 40 pmol labelled TTA G-quadruplex forming oligonucleotide using lipofectamine 2000, and then incubated with 5 μM 9Cl for 2 hours. (A) Fluorescence signal collected between 655-755 nm at λ_{ex} = 635 nm, (B) fluorescence signal collected between 425-470nm at λ_{ex} = 405 nm, (C) fluorescence signal collected between 500-545nm at λ_{ex} = 405 nm, (D) merged image of (B) and (C), (E) merged images of (A), (B), (C) and bright field. Scale bar, 20 μm.

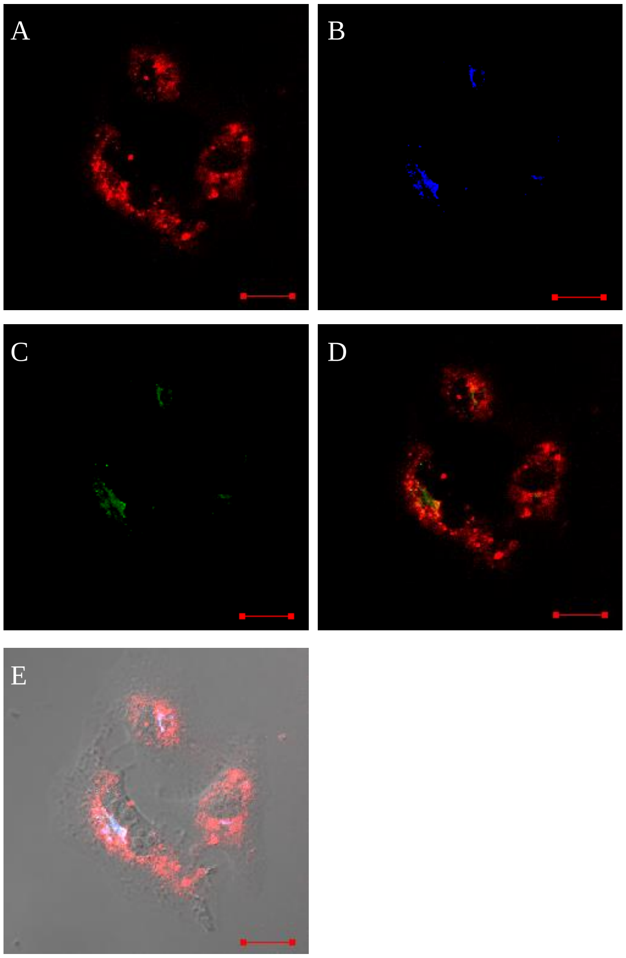

Figure S11. Fluorescence images of A549 cells transfected with 40 pmol labelled *c-KIT*1 G-quadruplex forming oligonucleotide using lipofectamine 2000, and then incubated with 5 μM 9Cl for 2 hours. (A) Fluorescence signal collected between 655-755 nm at λ_{ex} = 635 nm, (B) fluorescence signal collected between 425-470nm at λ_{ex} = 405 nm, (C) fluorescence signal collected between 500-545nm at λ_{ex} = 405 nm, (D) merged image of (B) and (C), (E) merged images of (A), (B), (C) and bright field. Scale bar, 20 μm.

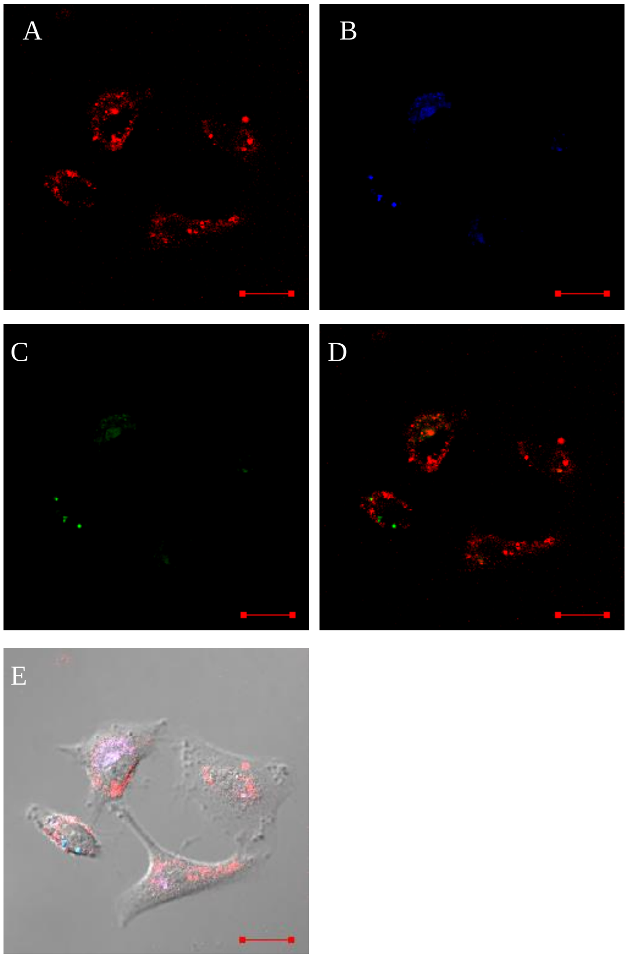

Figure S12 Fluorescence images of A549 cells transfected with 40 pmol *c-MYC* Pu22 G-quadruplex forming oligonucleotide labelled with Cy3 using lipofectamine 2000, and then incubated with 5 μM 9Cl for 2 hours. (A) Fluorescence signals at λ_{ex} = 405 nm, λ_{em} = 500-545 nm; (B) fluorescence signals at λ_{ex} = 405 nm, λ_{em} = 570-625nm (Cy3); (C) merged image of (A),(B) and bright field; (D) image of 9CI prior to photobleaching of the acceptor Cy3 (insert), (E) the fluorescence enhancement of 9CI after Cy3 was photobleached (insert), (F) FRET efficiency measured with the donor quenching approach，and the color bar represents the FRET efficiency. Scale bar, 10 μm.

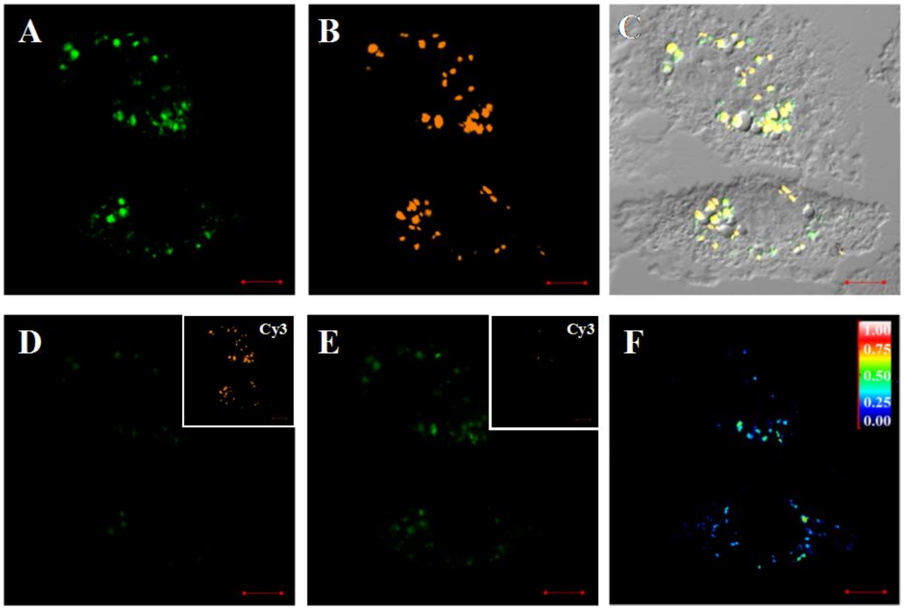

FRET between 9CI and Cy3 could provide direct evidence for the recognition between them. According to the emission spectrum of complex and the absorption spectrum of Cy3, FRET could happen between 9CI and Cy3. After the Cy3 labeled *c-MYC* Pu22 and 9CI were transfected to A549 cells, at the excitation wavelength of 9CI, the fluorescence signals collected between 500 nm and 545 nm (Figure S12A) showed the location of 9CI, and the fluorescence signals collected between 570 nm and 625nm suggested the FRET happen between 9CI and Cy3 (Figure S12B).

A donor dequenching approach was employed to validate FRET between 9CI and Cy3. Fluorescence intensity of 9CI was measured before and after the photobleaching of the Cy3 acceptor. The FRET efficiency was calculated as E= (DQ-Q/DQ), where DQ is the fluorescence intensities at the dequenched state, and the Q is the fluorescence intensities at the quenched state. Compared with the fluorescence intensity of 9CI at the quenched state, the increased fluorescence intensity of 9CI at the dequenched state further proved the existence of FRET between 9CI and Cy3 (Figure S12 D-F). Prebleach and postbleach images were taken serially with lower laser intensity.

Figure S13. Fluorescence spectra of solution at λ_{ex} = 405 nm.1) 1 μM 9CI (black line); 2) 1 μM 9CI and 0.5 μM *c-MYC* Pu22 DNA (red line); 3) 1 μM 9CI, 0.5 μM *c-MYC* Pu22-MFP DNA and 0.5 μM SL1-M (blue line).

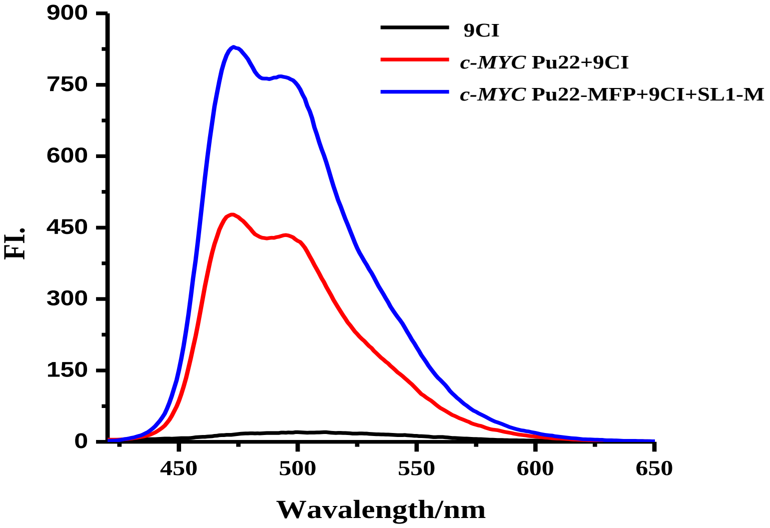

Figure S14. Confocal microscopy images of the treated A549 cells and HEK293T cells at 405 nm excitation for locating AS1411. Cells was incubated with AS1411-M for 30 min at room temperature, and washed by 1 mL DPBS twice. Then, the cells were incubated with 500 nM MFP (*c-MYC* Pu22-MFP/TTA-MFP) and 5μM 9CI for 10 min. Fluorescence signals were collected after the cells were washed with DPBS three times again. (A) Fluorescence signals collected at 425-470 nm emission channel, (B) fluorescence signals collected at 500-545 nm emission channel, (C) merged image of (A) and (B) and bright field. Scale bar, 10 μm.

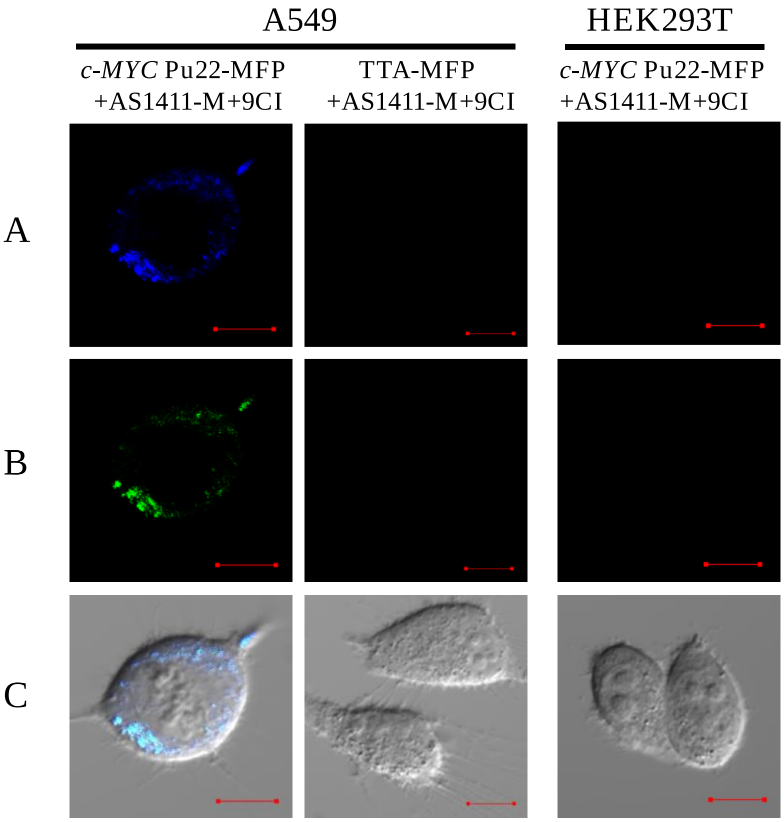

Figure S15. Job plot analysis for the binding stoichiometry of 9CI to *c-MYC* Pu22 G-quadruplex in 10 mM KH_2PO_4/K_2HPO_4 buffer (pH 7.0) with 100 mM KCl at room temperature. The sum of the concentration of 9CI and the concentration of *c-MYC* Pu22 G-quadruplex-forming oligonucleotide was fixed at 2 μM. The fluorescence intensity was plotted against molar ratio of [9CI]/([9CI] + [DNA]). The excitation wavelength was set at 405 nm, and the emission was collected at 472 nm. The intersection point is near 0.5, where 9CI exhibits binding of 1:1 stoichiometry to *c-MYC* Pu22 G-quadruplex.

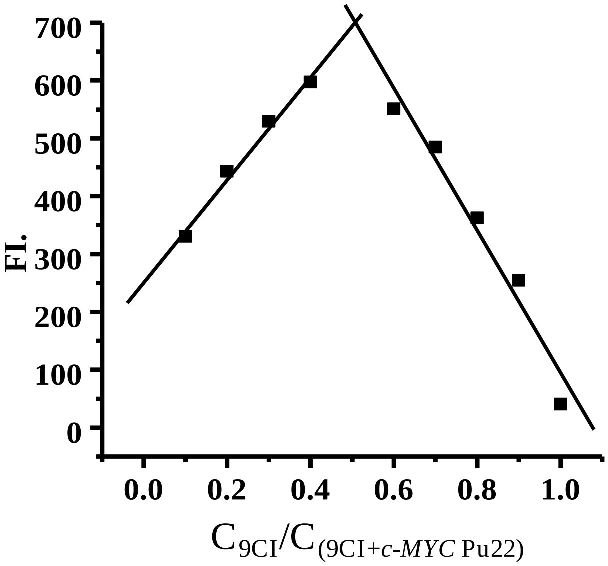

Figure S16. ITC binding isotherm of 20 μM 9CI interacting with 150 μM *c-MYC* Pu22 G-quadruplex DNA. This experiment was performed in buffer with 100 mM KCl, 10 mM KH_2PO_4/K_2HPO_4 (pH 7.0) at 25 °C.

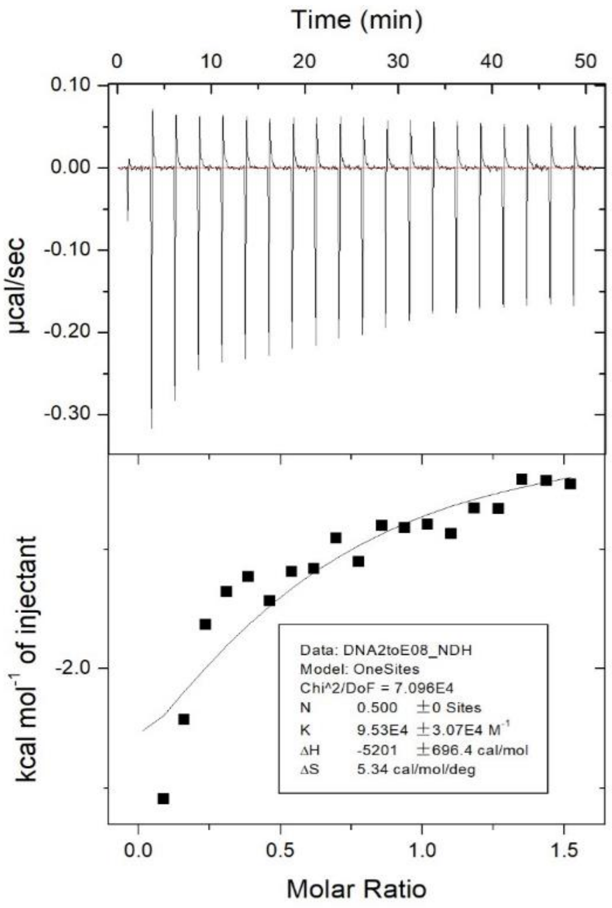

Figure S17. Linear relationship of fluorometric titration. Benesi-Hildebrand plot of 1/(F-F_0) versus 1/[DNA]. The Ka value was calculated as 8.33 x 10^5 M^{-1} for the binding between *c-MYC* Pu22 G-quadruplex and 9CI.

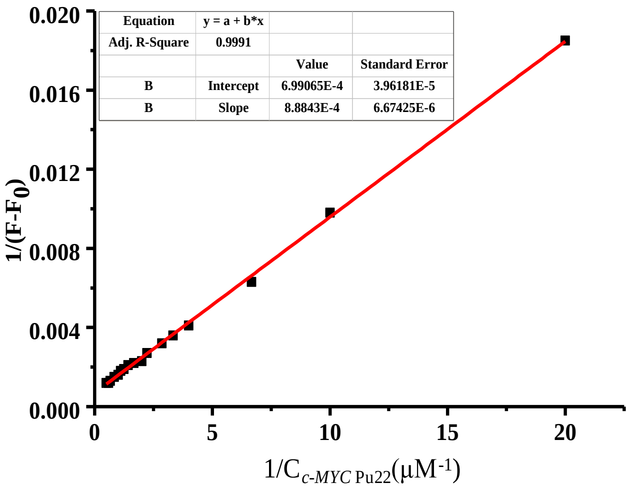

Figure S18. CD spectra of 10 μM G-quadruplex-forming oligonucleotides *c-MYC* Pu22, *c-KIT1*, TTA, TBA and CT4 in 10 mM KH_2PO_4/K_2HPO_4 buffer, 100 mM KCl, pH 7.0, with/without 20 μM 9CI at room temperature.

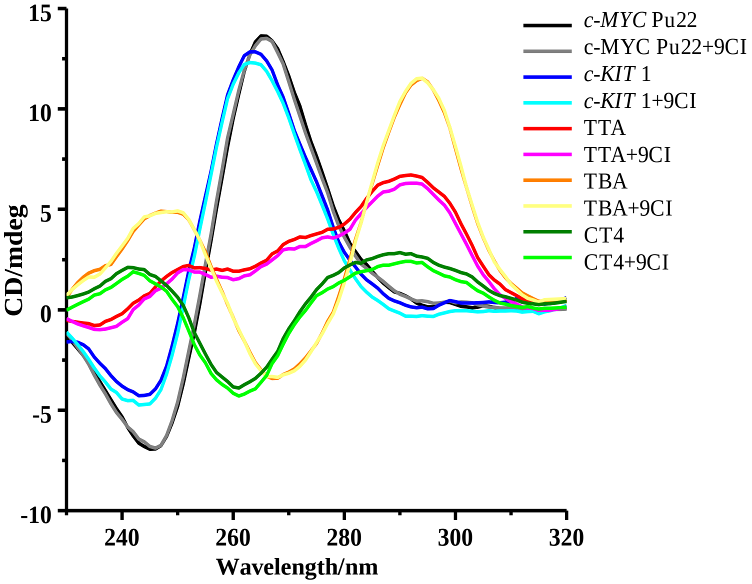

Figure S19. CD spectra of 10 µM *c-MYC* Pu22 DNA G-quadruplex oligonucleotide and the mutated oligonucleotides: *c-MYC* Pu22 G2>C2, *c-MYC* Pu22 T11>A11, *c-MYC* Pu22 T20>A20, *c-MYC* Pu22 A22>T22, *c-MYC* Pu22 A3>T3, *c-MYC* Pu22 G10>T10 in 10 mM KH_2PO_4/K_2HPO_4 buffer, 100 mM KCl, pH 7.0, with/without 20 µM 9CI at room temperature.

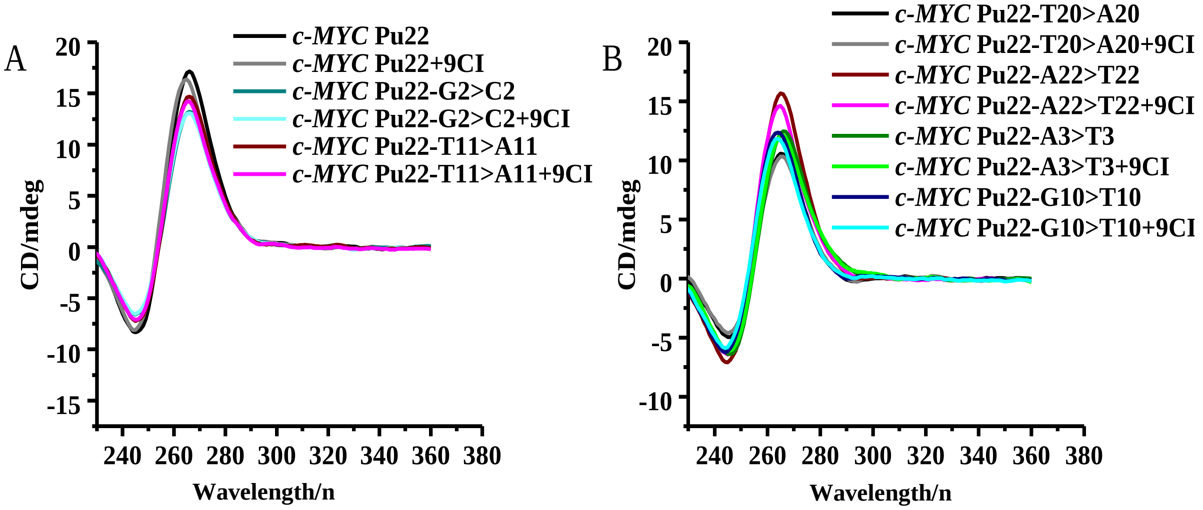

Figure S20. Binding model of 9CI in the 3' end cleft of *c-MYC* Pu22 G-quadruplex as predicted by Autodock 4.0. G-quadruplex is in yellow stick, and 9CI is in green. Figure S20B was obtained by rotating 90° from Figure S20A.

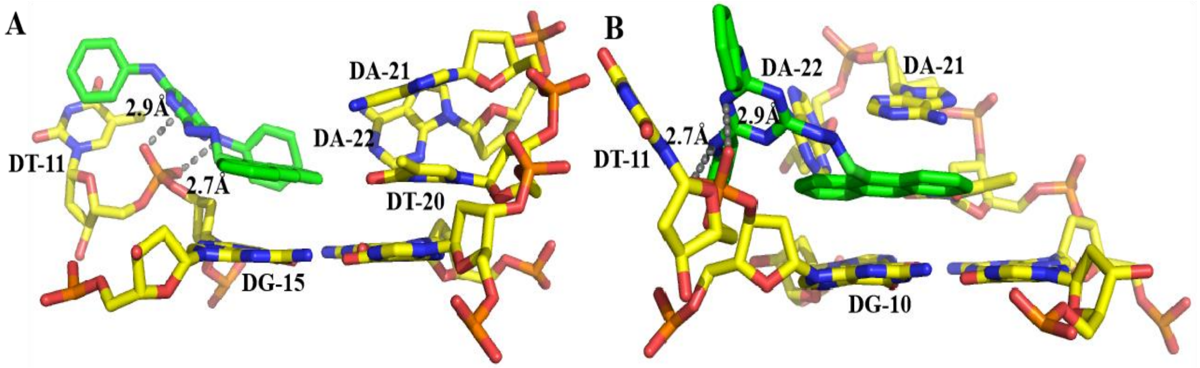

Figure S21. (A) RMSD of nucleic acid backbone in *c-MYC* Pu22 G-quadruplex structure over the course of the molecular dynamic simulation between 9CI and *c-MYC* Pu22 G-quadruplex. The inset structures highlight the conformation of binding at 100ns, 300ns, 500ns, 700ns and 1000ns. (B) Distance between C1' atoms of G19 and T20; (C) distance between C1' atoms of T20 and A22. (D) Conformational flexibility of the T20-A21-A22 loop observed over the course of the simulation. The figure illustrates 20 structures extracted every 50 ns. The conformation of the ligand (yellow) and the rest of the G-quadruplex is a snapshot taken at 1000 ns.

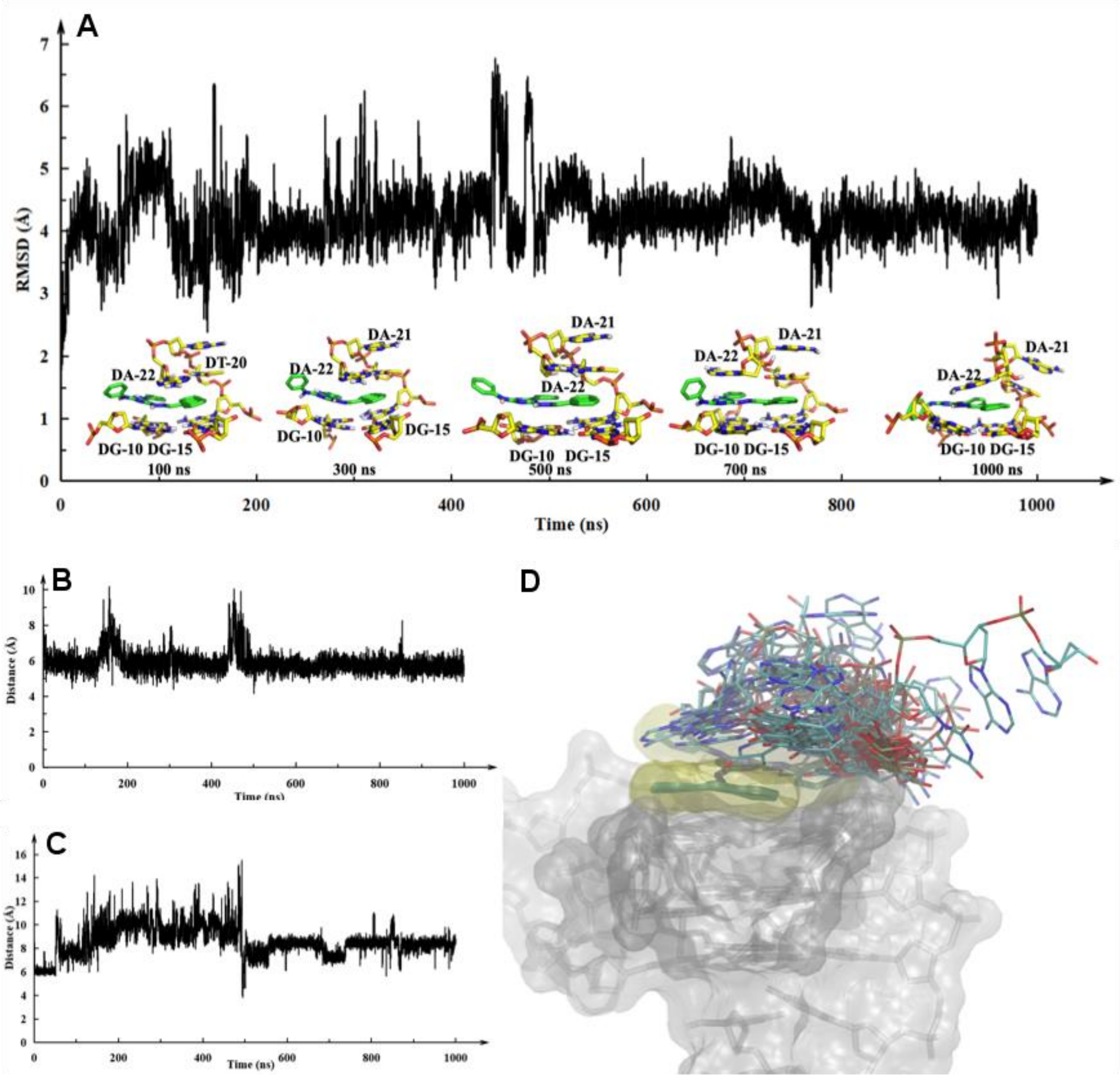

Figure S22. Binding modes of 9CI in the 3' end cleft of *c-MYC* Pu22 G-quadruplex explored by molecular dynamics simulation. Three figures are in different orientation.

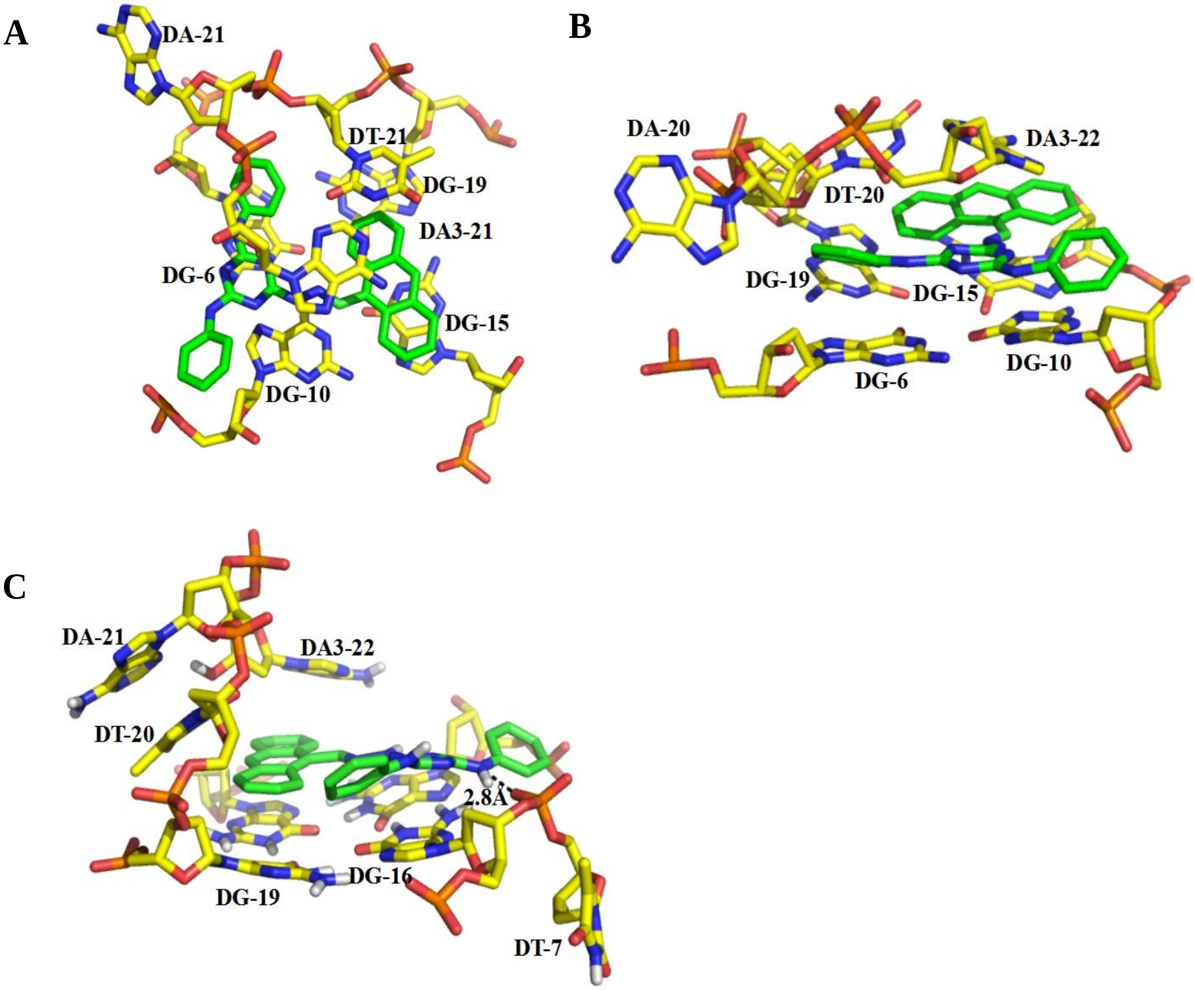

Figure S23 Fluorescence intensity variance of 9CI (1 μM) in buffer (10mM K_2HPO_4/KH_2PO_4 with 100 mM KCl at pH 7.0) with glycerol at different concentrations.

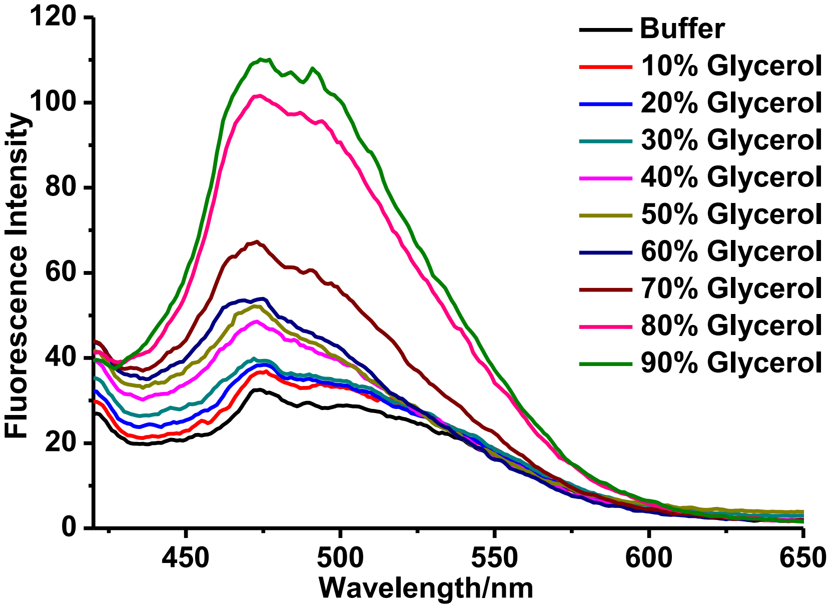

Figure S24 1D ^{1}H NMR spectra of *c-MYC* Pu22 G-quadruplex DNA mixing with d6-DMSO at different ratios (V/V).